Computer Methods and Programs in Biomedicine 209 (2021) 106315

Contents lists available at ScienceDirect

Computer Methods and Programs in Biomedicine

journal homepage: www.elsevier.com/locate/cmpb

Bone collision detection method for robot assisted fracture reduction based on force curve slope

Chenxu Cai[a,b], Congyu Sun[a,b], Yixuan Song[a,b], Qinjing Lv[a,b], Jianping Bi[c], Qinhe Zhang[a,b,*]

[a] Key Laboratory of High Efficiency and Clean Mechanical Manufacture (Ministry of Education), School of Mechanical Engineering, Shandong University, Jinan 250061, China
[b] National Demonstration Center for Experimental Mechanical Engineering Education, Shandong University, Jinan 250061, China
[c] The Affiliated Hospital of Shandong University of Traditional Chinese Medicine, China

ARTICLE INFO

Article history:
Received 22 April 2021
Accepted 21 July 2021

Keywords:
Bone fracture reduction
Viscoelastic model
Collision detection model
Force detection
Slope ratio

ABSTRACT

Background and objective: The application of robot technology in fracture reduction ensures the minimal invasiveness and accurate operation process. Most of the existing robot assisted fracture reduction systems don't have the function of bone collision detection, which is very important for system safety. In view of the deficiencies in the research of this field, a broken bone collision detection method based on the slope ratio of force curve was proposed in this paper, which could realize the real-time detection.

Methods: In order to analyze the factors influencing the slope of force curve, a collision mechanical model based on three-element viscoelastic model was established. The effects of four factors on the slope ratio of the force curve were studied based on the mechanical model. The proposed collision detection model was analyzed in detail. By drawing slope ratio curves under various experimental conditions, the universality of the collision detection model was proved; by comparative simulation, the differences between the slope ratio curves before and after optimization were analyzed. The factors that affect the performance of the detection model were also analyzed.

Results: The results of collision experiments show that the increase of moving speed of distal bone and soft tissue mass reduces the slope ratio, while the increase of collision angle increases the slope ratio. In the verification experiment, the minimum main peak of KR_{opt} curve is 14.16 and the maximum is 220.7, the maximum interference value before the peak is 6.1. When the detection threshold is 10, the model can detect the collision state of the broken bone. It is also proved that after optimization, the model can effectively filter out invalid waveforms and reduce the occurrence of false detections. When a=5 and b=40, the detection model has sufficient stability and a low detection time delay.

Conclusion: This research developed a broken bone collision detection method based on the slope ratio of the force curve. After optimization, the method has good adaptability under a variety of experimental conditions. The collision of broken bones can be judged by setting an appropriate detection threshold. The application of this method in the robot fracture reduction system will improve the safety of the system.

1. Introduction

The application of robot in fracture reduction surgery can achieve a more accurate reduction process under minimally invasive conditions [1,2]. At present, for the fracture reduction robot systems, the fracture bone is generally remodel based on CT images, and then the navigation system is used to determine the fracture position [3–6]. Besides, intraoperative registration [7], preoperative path planning [8,9] and other methods were used to achieve robot assisted fracture reduction by some researchers. However, no matter which method is used, the position of broken bone is non-intuitively expressed with the help of instruments. The surgical errors will be leaded inevitably by the insufficient performance of the instruments, such as the accuracy of 3D remodeling software, navigation system and robot. Therefore, in the process of fracture reduction, there is the risk of unexpected collision on both sides of the broken bone, which may cause irreversible damage to patients.

* Corresponding author.
E-mail address: zhangqh@sdu.edu.cn (Q. Zhang).

https://doi.org/10.1016/j.cmpb.2021.106315
0169-2607/

When the joystick is used to control the surgical robot, it seems to be a good choice for joystick to get feedback of the mechanical information detected by the robot end sensor in real time. This method can effectively reduce the risk of surgery [10,11]. At present, when the handle is used for control, it is always given the function of force feedback [12]. A number of studies have shown that, compared with no force feedback, devices with force feedback function can effectively improve the success rate of surgery and reduce the risk of surgery [13,14]. The application of force feedback handle in fracture reduction surgery has been studied [15,16]. The operator can judge whether the broken bones have collided with each other through the feedback force from the handle. However, this method is subjective. Besides, the reduction force in the process of fracture reduction is very large [17]. The operator cannot accurately obtain the mechanical characteristics of the broken bones when the bones collide. It is necessary to study more objective methods to accurately extract the mechanical characteristics and determine whether the broken bones have collided during the reduction process.

In fact, the force detection method has been applied in other types of surgical robots. For example, Ning et al. [18] applied multi-dimensional force sensor in lumbar robotic surgery system to judge the working state of the system and improve the safety of the system. Xue et al. [19] and Zhao et al. [13] both developed new end force detection method with good accuracy. Their studies reduced the impact of the narrow space at the end of the abdominal surgery robot and the sterilization process on the mechanical sensor. But there is only a little research on the detection of bone collision during fracture reduction now [20,21]. Kim et al. [22] proposed a force feedback scheme based on dual force torque sensor and adjustable admittance to prevent the positioning robot from exerting excessive force on the fracture bone, which is conducive to improving the safety of the operation process. However, there is still no exact and feasible method to detect whether the broken bones collide during the reduction process.

When the robot is used for fracture reduction, the robot holds the K-wires to realize the movement of the broken bone. As the mechanical properties of bone and surrounding soft tissue are very different [23,24], the clamping force of the manipulator will change significantly after the bones collision. Whether the broken bones are in contact with each other can be judged by detecting the force curve characteristics before and after the collision.

In this paper, a collision detection model based on the slope ratio of force curve is established by analyzing the mechanical model before and after the collision. The application method of this model in the system is also given. At last, the influence of different parameters on the performance of the detection model is investigated.

2. Collision detection model of fracture reduction

2.1. Mechanical model before and after collision

The mechanical properties of biological tissues are complex, the most obvious of which is viscoelasticity [25], while the three-element model can simultaneously express the relaxation and creep properties of viscoelastic materials [26]. Therefore, this paper chooses a three-element model composed of elastic elements in series with Kelvin model to represent the mechanical properties of soft tissues and bones. The relationship between force and deformation of the three-element model is shown in Fig. 1. The elastic modulus of the elastic element is K_2, the elastic modulus of the Kelvin model is K_1, and the damping coefficient isη. Assuming that the model is stretched in the initial state, and the initial tension is F_0. When the model is retracted, the force of the three-element model is equal to the elastic force of the elastic element, and at the same time equal to the force of the Kelvin model element. When the displacement L_1 of the intermediate node is eliminated, the relationship between the model force F and its deformation L can be obtained.

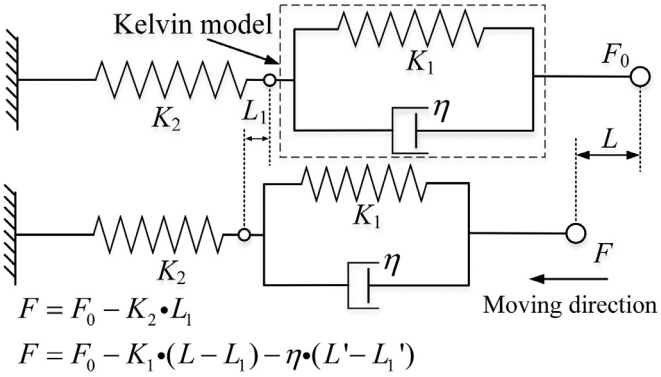

Fig. 1. Relationship between force and deformation of the three-element model

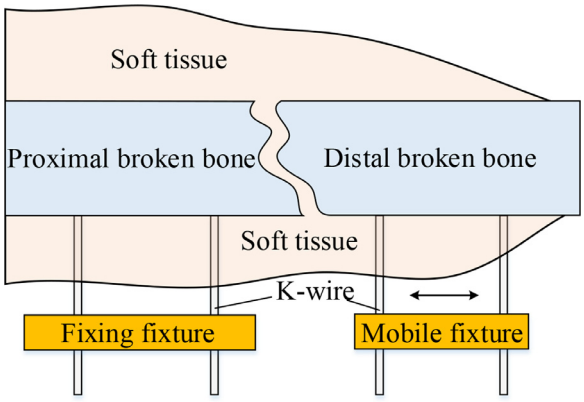

Fig. 2. The relative position of broken bones during reduction

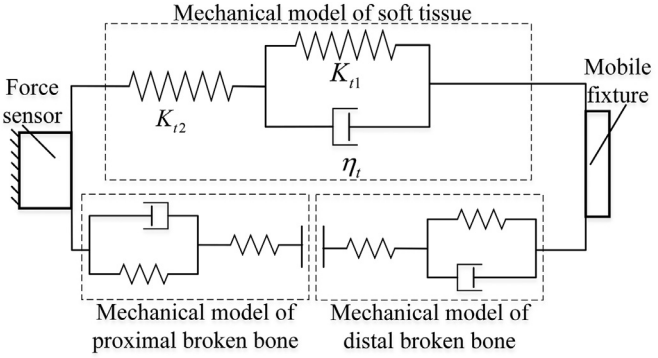

Fig. 3. Viscoelastic mechanical model before collision

In the process of reduction, the proximal broken bone is usually fixed. While the distal broken bone is pulled apart, and then gradually pushed back until the two broken bones contact each other. The relative position of the two sides of the broken bones in the reduction process is shown in Fig. 2, and the mechanical model before the collision is shown in Fig. 3, where K_{t1} and K_{t2} are the elastic coefficients of soft tissue, η_t is the viscosity coefficient of soft tissue.

Simplifying that K_{t1}=K_{t2}=K_t. When the distal broken bone is at the initial position, the distance between proximal and distal broken bones is L_0, and the initial force value is F_0. The horizontal right direction is the positive direction of the force. During the

whole reduction process, the soft tissue is in a stretching state. From Fig. 1, before the collision, the relationship between the force value detected by the mechanical sensor and the moving distance of the distal broken bone is shown in Eq.1.

$$F_0 - F(t) - \frac{\eta_t}{2K_t}\frac{dF(t)}{dt} = \frac{K_t}{2}L(t) + \frac{\eta_t}{2}\frac{dL(t)}{dt} \quad (t < t_0) \tag{1}$$

Where, $F(t)$ is the force value detected by the mechanical sensor, $L(t)$ is the movement distance of the distal broken bone, t is time, t_0 is collision time. Assuming that the distal broken bone moves at a constant speed and the speed is v. With the boundary condition $F(0)=F_0$, Eq.2 is obtained by solving the differential equation of Eq.1.

$$F(t) = F_0 - \frac{K_t v t}{2} - \frac{\eta_t v}{4}(1 - e^{-\frac{2K_t}{\eta_t}t}) \quad (t < t_0) \tag{2}$$

$$F'(t) = -\frac{K_t v}{2}(1 + e^{-\frac{2K_t}{\eta_t}t}) \quad (t < t_0) \tag{3}$$

After the collision, the broken bones on both sides are combined together. As the collision force is much larger than the soft tissue force, the force received by the force sensor at the moment of collision is similar to the collision force of broken bones. The soft tissue force can be ignored comparing with collision force, then $F(t_0)\approx 0$. After collision, the comprehensive stiffness coefficient is K_m, the comprehensive viscosity coefficient is η_m. In a short time after the collision, it is considered that the distal broken bone is still moving at a uniform speed, and the speed is v. The relationship between the force value detected by the force sensor and the moving distance of the distal broken bone is:

$$-F(t) - \frac{\eta_m}{2K_t}\frac{dF(t)}{dt} = \frac{K_m}{2}(vt - vt_0) + \frac{\eta_m}{2}v \quad (t > t_0) \tag{4}$$

The solution of the differential equation of Eq.4 is as follows:

$$F(t) = -\frac{K_m v(t - t_0)}{2} - \frac{\eta_m v}{4}(1 - e^{-\frac{2K_m}{\eta_m}(t-t_0)}) \quad (t > t_0) \tag{5}$$

$$F'(t) = -\frac{K_m v}{2}(1 + e^{-\frac{2K_m}{\eta_m}(t-t_0)}) \quad (t > t_0) \tag{6}$$

Since the calculation is the change of the collision force at the moment of the collision, then$t - t_0 \to 0$, the slope ratio of the force curve before and after the collision is:

$$KR = \frac{F'(t_0^+)}{F'(t_0^-)} = \frac{K_m}{K_t}\frac{2}{1 + e^{-\frac{2K_t}{\eta_t}t_0}} \tag{7}$$

It can be seen from Eq.7 that the slope ratio of the force curve before and after collision is related to a variety of factors, including the stiffness of soft tissue K_t, the comprehensive stiffness of broken bone and clamping device K_m and the viscosity coefficient of soft tissue η_t. The collision time t_0 also affect the value of the slope ratio.

2.2. Collision detection model based on slope ratio

According to the analysis in Section 2.1, the focus of this paper is to study a slope comparison method of force curves. The purpose of this method is to realize real-time collision detection. In the actual operation process, the force data collected by the system is a series of discrete points.

In this paper, the newly collected data point P_{new} is selected as the benchmark. P_a is obtained by selecting a data length point backward, and P_b is obtained by selecting b data length point backward further. As is shown in Fig. 4, taking the data points of P_b-P_a and P_b-P_{new} as the comparison object, the slope values of the two sections are obtained by linear fitting method.

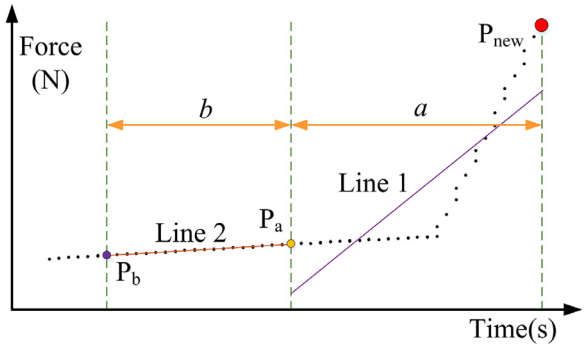

Fig. 4. Data point selection and fitting

In Fig. 4, Line1 is the straight line obtained by linear fitting of data points in section P_a-P_{new}, and Line2 is the straight line obtained by linear fitting of data points in section P_b-P_a. The least square method is used to obtain the linear regression equation of data points. The slope can be expressed by Eq.8:

$$K = \frac{\sum t_i F_i - \sum t_i \sum F_i/n}{\sum t_i^2 - (\sum t_i)^2/n}(i = 1, 2, \ldots, n) \tag{8}$$

Where K is the slope; n is the number of data points; t_i is the abscissa of point i; F_i is the force value detected at time t_i. The standard deviation of the linear slope K is:

$$S(K) = \sqrt{\frac{1}{n-2}\frac{\sum (F_i - \hat{F}_i)^2}{\sum (t_i - \sum t_i/n)^2}}(i = 1, 2, \ldots, n) \tag{9}$$

Where, $\hat{F}_i (i = 1, 2, \ldots, n)$ is the force obtained after linear fitting. It can be seen from Eq.9 that the data length n affects the stability of the slope of the straight line. In order to ensure the stability of the fitting and the sensitivity of detection, an appropriate data length should be selected.

According to the above analysis, the objective function of the detection model is shown in Eq.10. Where, $K_{b\text{-}a}$ is the slope value of section P_b-P_a after fitting, and $K_{a\text{-}new}$ is the slope value of section P_a-P_{new} after fitting. However, in the actual reduction process, it is difficult to achieve uniform speed. In this way, the slope value of section P_b-P_a may be very small or equal to zero. Even if no collision occurs in section P_a-P_{new}, it is possible that the slope ratio is very large. The collision state will be misjudged when using Eq.10. Therefore, the objective function is further restricted in this paper. The optimized objective function is shown in Eq.11.

$$KR(i) = \frac{K_{a-new}(i)}{K_{b-a}(i)}(i = 1, 2, \ldots) \tag{10}$$

$$\begin{cases} KR_{opt}(i) = \frac{K_{a-new}(i)}{K_{b-a}(i)} & |K_{b-a}(i)| \geq A \\ KR_{opt}(i) = 0 & K_{b-a}(i) \cdot K_{a-new}(i) < 0 \\ KR_{opt}(i : i + b - 1) = 0 & |K_{b-a}(i)| < A \end{cases} \quad (i = 1, 2, \ldots) \tag{11}$$

Where, KR_{opt} is the slope radio after optimization, A is the preset minimum threshold. The reference value can be obtained by the tensile test with the soft tissue of the minimum strength as the experimental object at the minimum movement speed of the system. The meaning of Eq.11 is shown in Fig. 5.

When it is detected that the $K_{b\text{-}a}(i)$ is less than A, the P_b-P_a segment is considered to be horizontal, and the values of $KR_{opt}(i,i+1,\ldots,i+b-1)$are set to 0 regardless of the value of $K_{b\text{-}a}$ $(i,i+1,\ldots,i+b-1)$ and $K_{a\text{-}new}$ $(i,i+1,\ldots, i+b-1)$. When calculating $KR_{opt}(i+b)$, if the value of $K_{b\text{-}a}(i+b)$ is still less than A, the above steps will be repeated until it is more than or equal to A. When the changing trends of the force curves before and after the collision are inconsistent, the collision will not occur, so the KR_{opt} value is also set to 0 in this case.

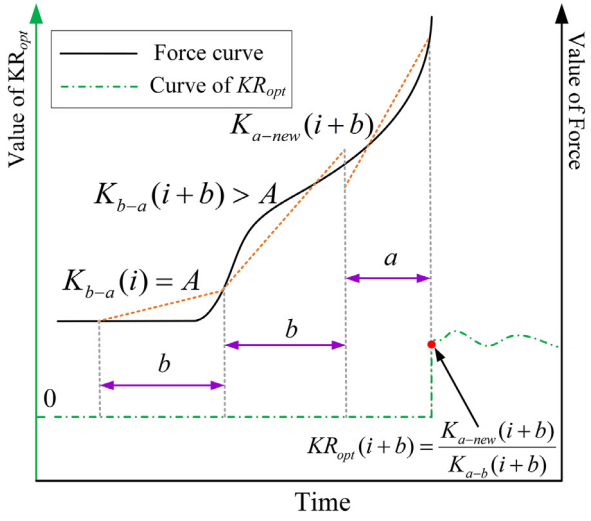

Fig. 5. Calculation diagram of objective function

3. Experiments and methods

3.1. Experimental device

In order to verify the mechanical model and collision detection model, collision experiments are carried out. When the collision detection model is applied to a robot-assisted fracture reduction system, it is necessary to install a force sensor on the end of the robot or the fixation device of the proximal broken bone to detect the value of the reduction force in real time. A feasible reduction strategy of the robotic reduction system is shown in Fig. 6. The collision detection model is mainly used in the fourth step of the process. According to the work of the fourth step, the experimental device was built, and its structure is shown in Fig. 7.

In the fourth step, the robot drives the distal broken bone to move in a straight line along the axis of the broken bone, so linear motor is used as a driving device in the experiment. Four fresh porcine femurs were selected as the broken bones for the experiment, and they were used in four different experiments. Each of the porcine femurs was cut into two equal length segments. One segment was installed on the fixing fixture by K-wire as the proximal broken bone, the other segment was fixed on the mobile fixture by K-wire as the distal broken bone. The mobile fixture could move by the linear motor. Fresh porcine femurs muscle was used as soft tissue material. The muscle fibers were trimmed into uniform strips with scalpel. The length of all muscle strips was within

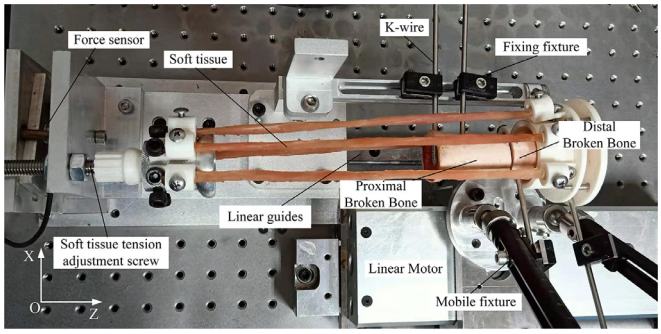

Fig. 7. Experimental device

20±0.5cm and the weight was within 6±0.2g. The two ends of the muscle strip were fixed on the distal broken bone and the adjusting screw, respectively. The model of the force sensor was ATI Nano-17, with Z-direction measurement range of ±35N and resolution of 1/160N. As shown in Fig. 7, the horizontal right direction is the Z-direction of the force sensor. The force data was collected and saved by LABVIEW at a sampling frequency of 100Hz. The data was processed by MATLAB.

3.2. Experimental parameters

It can be seen from Eq.7 that the factors affecting the slope ratio mainly include the stiffness of soft tissue, the viscosity coefficient of soft tissue, the stiffness of fracture bone and clamping device, etc. The stiffness and viscosity coefficient were changed by changing the mass of soft tissue. The stiffness of the broken bone was changed by changing the area of the collision surface. In addition, the actual collision is not necessarily a frontal collision. The angle between the collision surfaces may affect the result, so the influence of collision angle on the force curve was also studied. Although the influence of reduction speed on *KR* cannot be shown directly from Eq.7, the speed will affect the value of t_0. Therefore, the influence of reduction speed on *KR* was also studied.

Four groups of single factor experiments were designed to study the effects of soft tissue mass, collision surface area, collision angle and reduction speed on *KR*. The experimental parameters are shown in Table 1-4.

3.3. Experimental methods

As shown in Fig. 8, the collision side of the proximal broken bone is trimmed to a boss with a height of 25mm and a variable

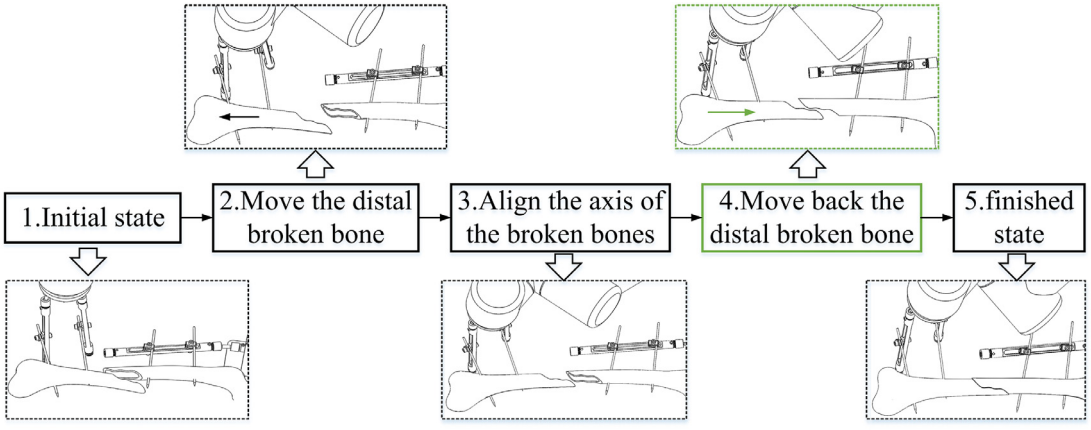

Fig. 6. A feasible reduction strategy of the robotic reduction system

Table 1
Changes in soft tissue mass

Experiment number	Mass of soft tissue(g)	Collision surface area(mm^2)	Collision angle (in degree)	Reduction speed(mm/s)
1	6	12	90	1
2	12	12	90	1
3	18	12	90	1
4	24	12	90	1
5	30	12	90	1
6	36	12	90	1

Table 2
Changes in the area of collision surface

Experiment number	Mass of soft tissue(g)	Collision surface area(mm^2)	Collision angle (in degree)	Reduction speed(mm/s)
1	24	12	90	1
2	24	24	90	1
3	24	36	90	1
4	24	48	90	1

Table 3
Changes in collision angle

Experiment number	Mass of soft tissue(g)	Collision surface area(mm^2)	Collision angle (in degree)	Reduction speed(mm/s)
1	24	12	30	1
2	24	12	50	1
3	24	12	70	1
4	24	12	90	1

Table 4
Changes in reduction speed

Experiment number	Mass of soft tissue(g)	Collision surface area(mm^2)	Collision angle (in degree)	Reduction speed(mm/s)
1	24	12	90	1
2	24	12	90	3
3	24	12	90	5
4	24	12	90	7
5	24	12	90	9

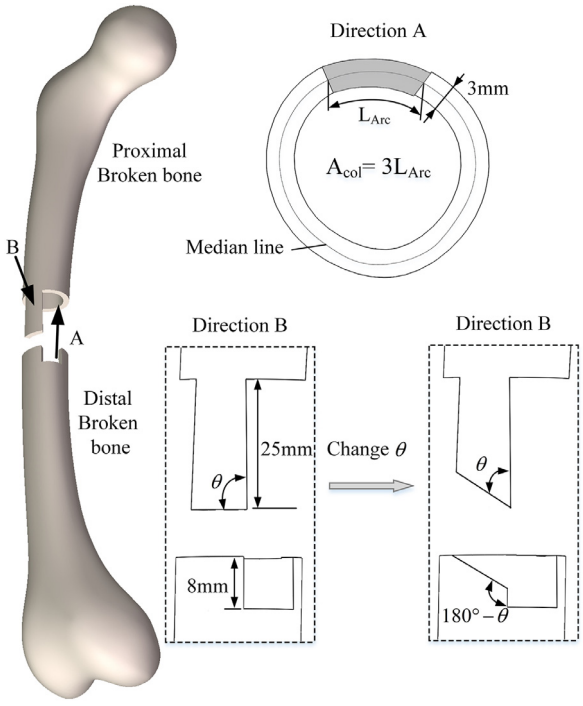

Fig. 8. Geometric parameters of collision location

width. According to the measurement, the cross-section of the broken bone can be approximately regarded as a ring with an average thickness of 3mm, and the cross-sectional area A_{col} of the boss can be changed by changing the length of the median line L_{Arc}. When changing the collision angle θ, the collision surface of the distal broken bone will also be adjusted to be parallel to the collision surface of the proximal broken bone.

At the beginning of the experiment, the collision surfaces of the proximal and distal broken bone were about to contact, and the contact force was zero. The initial tension of soft tissue was set as F_{start}=0.8n_t (N), where n_t is the number of soft tissue strips. After moving the distal broken bone to the right by 4 mm at a constant speed, the Z-direction force of the sensor was recorded. During the reduction process, the distance from the distal broken bone to the proximal was set to be 5mm, and the curve of soft tissue force and collision force during the reduction process was finally obtained.

4. Results and discussion

4.1. Results and discussion of single factor experiments

One of the experimental force curves is shown in Fig. 9 (a). In order to study the influence of different experimental parameters on the slope ratio of the force curve before and after the collision, the inflection point of the curve is selected as the reference point in MATLAB, and 20 points are taken on the left and right sides respectively. Finally, the slope values of the two fitting lines are obtained, as shown in Fig. 9. After the slope value is obtained, the

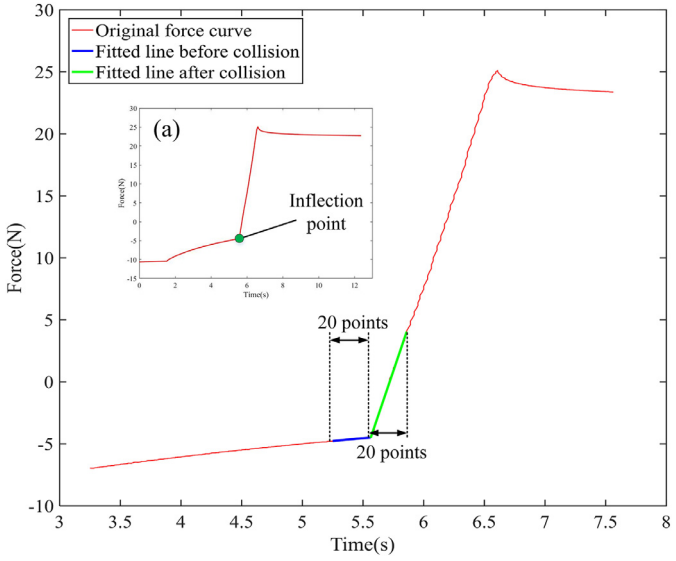

Fig. 9. Experimental force curve and fitting line

slope ratio can be obtained through dividing the slope after collision by the slope before collision.

The influence of various parameters on the slope ratio of the force curve is shown in Fig. 10. In order to explain the cause of the influence better, the slope of the fitting curve before and after the collision is also shown in this figure. In Fig. 10, K1 is the slope of fitting curve after collision and K2 is the slope of fitting curve before collision. As K1 is much larger than K2, in order to show them in the same figure, the value of the points on the curve after collision in the figure are 20 times larger than those of K2.

The data in Fig. 10 (a) shows that the slope ratio decreases with the increase of soft tissue mass. When the soft tissue mass increases by 6 times, K2 increases to 5.6 times and the slope ratio decreases to 15.7%. This is because with the increase of soft tissue mass, the stiffness of soft tissue also increases. K2 is mainly affected by the stiffness of soft tissue, and they are roughly positively correlated. K1 is less affected by soft tissue stiffness. So when the soft tissue mass increases, the slope ratio will decrease.

Table 5
Comparison of slope ratio curve parameters before and after optimization

Experiment Number	Before optimization NIP	MIP	VTP	After optimization NIP	MIP	VTP
1.1	7	1883	220.7	0	0	220.7
1.3	4	53	69.3	0	0	69.3
1.5	1	20.96	46.2	1	6.1	46.2
2.1	1	54.29	37.78	0	0	37.8
2.3	2	66.52	41.77	0	0	41.8
3.1	2	196.3	15.42	0	0	15.4
3.3	1	53.91	37.19	0	0	37.2
4.1	1	60.21	23.16	0	0	23.16
4.3	1	1867	21.97	0	0	22
4.5	1	235.6	14.16	0	0	14.16

It can be seen from Fig. 10 (b) that the slope ratio increases first and then decreases as the collision area increases. When the collision area is larger, the slope ratio decreases more mainly because the soft tissue stiffness is larger at this time. The experiment with larger area is done first when the strength of soft tissue is higher. With the increase of stretching times, the creep of soft tissue leads to the decrease of stiffness. However, the stiffness of the broken bone and the clamping mechanism does not change significantly, which may be due to the high strength of the bone. In the case of frontal collision, the stiffness does not decrease significantly when the cross-sectional area is 12mm^2.

As can be seen from Fig. 10 (c), when the collision angle changes from 30 to 90 in degrees, the slope ratio increases by 2.7 times. It can be seen from Fig. 8 that the shape of the boss at the proximal broken bone is relatively slender, and the lateral stiffness is smaller. When the collision angle is small, the deformation of the collision part is mainly lateral deformation, and the collision force will be smaller. Therefore, the slope ratio increases with the increase of collision angle.

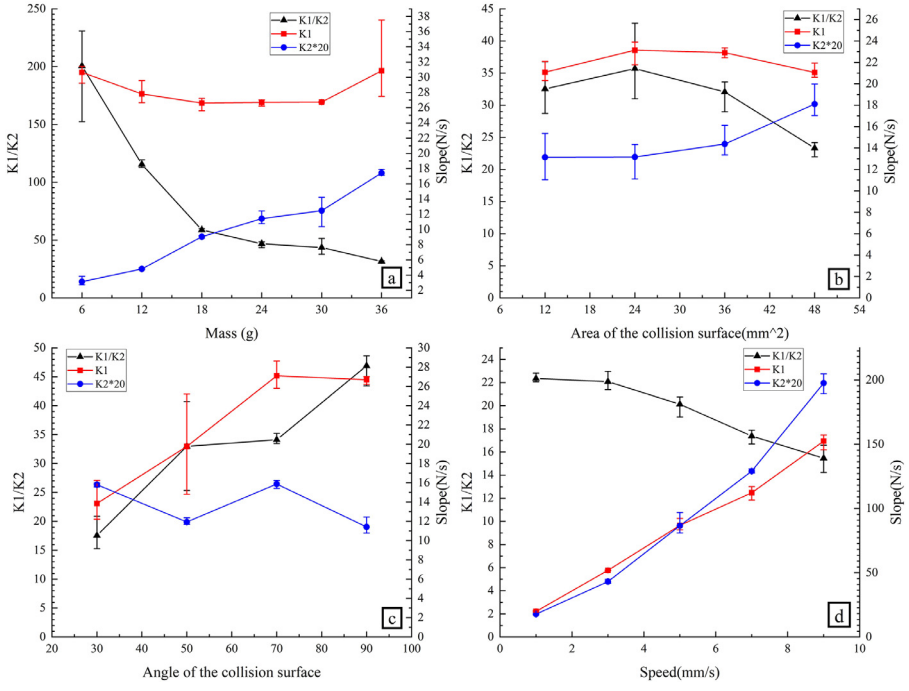

Fig. 10. The effect of experimental parameters on the slope and ratio of the curve

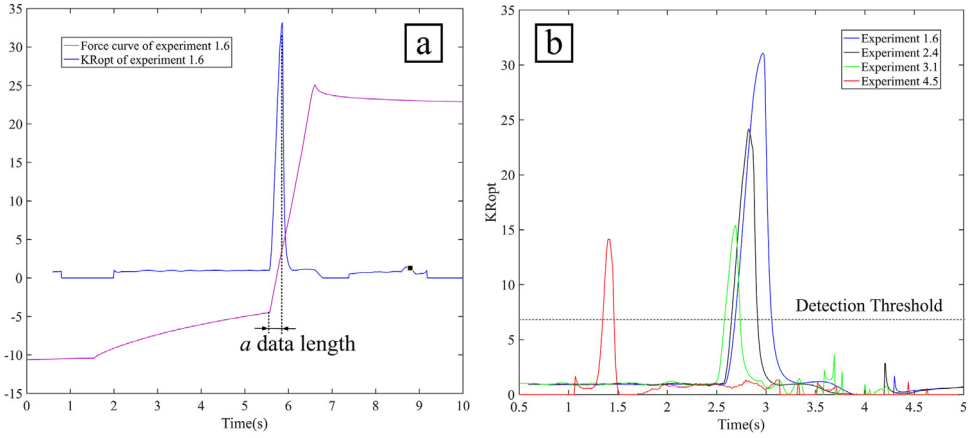

Fig. 11. Slope ratio model curve

As can be seen from Fig. 10 (d), with the increase of reduction speed, the slope ratio gradually decreases. When the speed increases by 9 times, the slope ratio becomes 70% of the initial value. After the collision, the value of K1 mainly depends on the stiffness of the broken bone and the clamping device. When the speed increases proportionally, the value of K1 also increases linearly, which is consistent with Fig. 10 (d). However, it can be seen from Eq.7 that the value of K2 not only depends on the stiffness of soft tissue, but also the time t_0 when the viscosity coefficient of soft tissue can't be ignored. The greater the reduction speed, the smaller the t_0 and the faster the increase of K2. Therefore, the slope ratio will decrease with the increase of reduction speed.

4.2. Verification of collision detection model based on slope ratio

Through the results and discussion in Section 4.1, the influence of various factors on the slope ratio is analyzed. In this section, the established collision detection model is verified according to the force curves obtained from the experiments. Under the condition of setting a=b=20, the force curve with the smallest slope ratio under each factor is selected as the research object.

The collision detection model curves are shown in Fig. 11. In this figure, the length of some curves is trimmed to be better compared. Where KR_{opt} is the value of the objective function in Eq.11. The label in the legend represents the experiment number of the curve. For example, Experiment 1.6 represents the 6th experiment with the 1st factor, corresponding to Table 1-4 in Section 3.2.

It can be seen from Fig. 11 (b) that there are obvious main peaks in the four curves. In order to detect the collision of broken bones, the detection threshold should be set, that is, when the value of KR_{opt} reaches the detection threshold, it is considered that the collision of broken bones has occurred. The peak value in Experiment 1.6 is the smallest, the detection threshold should be less than this value. Under the experimental conditions of this paper, the collision of broken bones can be reliably detected when the value of detection threshold is around 10. It can be seen from Fig. 11 (a) that the position of the main peak is near the collision point. The inherent characteristic of this collision detection model makes the detected collision time be a data length later than the actual collision time, that is, the main peak point is a data points later than the inflection point of the force curve.

In order to illustrate the advantages of the objective function Eq.11 over Eq.10, a force curve is constructed based on the data of single factor experiment 1.4 to simulate the irregular motion of the distal fractured bone before collision. As can be seen from Fig. 10 (a), the minimum value of K2 in this paper is 0.15. The threshold A should be less than this value, A is set to be 0.1. The

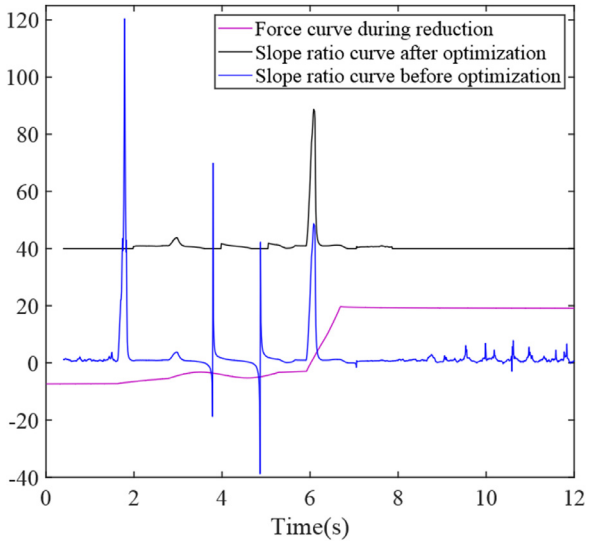

Fig. 12. Comparison of slope ratio curves before and after optimization

change of slope ratio curve before and after optimization is shown in Fig. 12. As the curves before and after optimization are highly overlapped in some positions, the optimized curve is translated up 40 unit lengths. Fig. 12 shows that, after optimization, the position and value of the slope ratio curve peak are not affected while clutter at special points is filtered out.

The generality of the optimized model under the experimental conditions is given in Table 5. The force curves of the above experiments are selected, and the KR curve and KR_{opt} curve are drawn respectively. The difference of the slope ratio curve before and after optimization can be obtained by comparing the characteristic parameters. In Table 5, NIP is the number of interference wave peaks, MIP is the maximum value of interference wave peak, and VTP is the value of the target wave peak. It should be noted that only peaks with a value greater than 5 are calculated. It can be seen from Table 5 that the optimized algorithm can well filter out interference waves without affecting the value of the target wave crest, which is beneficial to ensure the success of detection. As the maximum interference peak after optimization is 6.1, the impact of interference can be avoided when the detection threshold is 10.

According to the analysis in Section 2.2, in Eq.9, the data length n affects the stability of the slope of the straight line. In the detection model, a and b are the data lengths of the two fitting straight

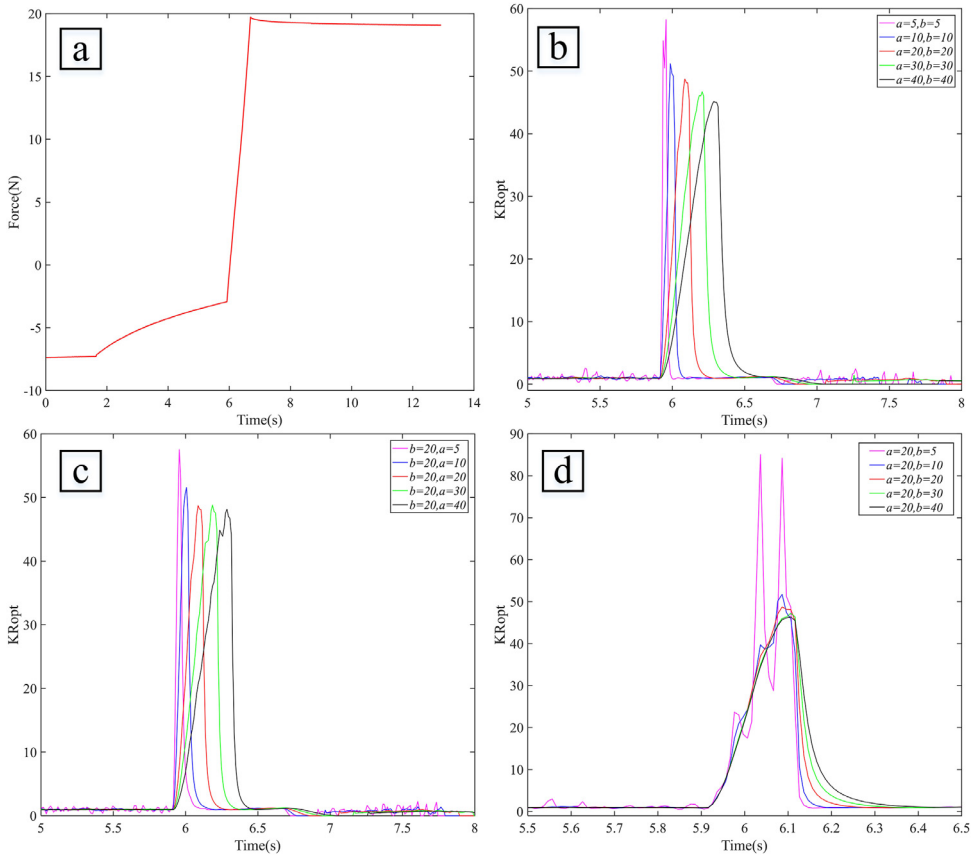

Fig. 13. The influence of a and b on KR_{opt}

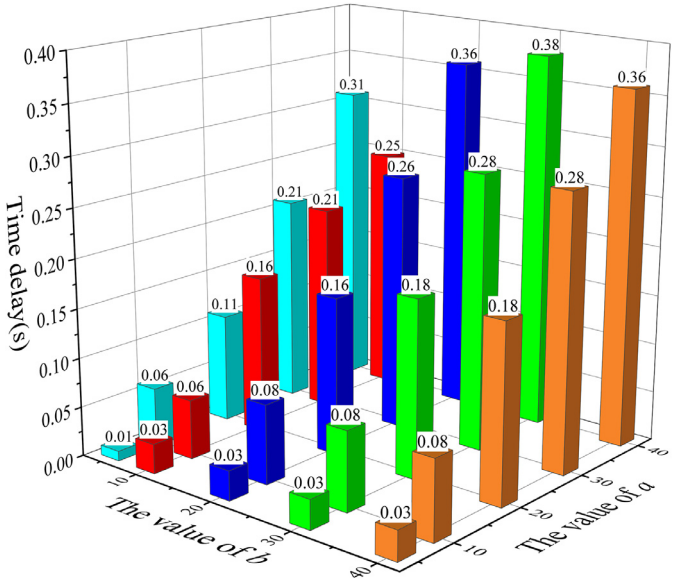

Fig. 14. The influence of a and b on time delay

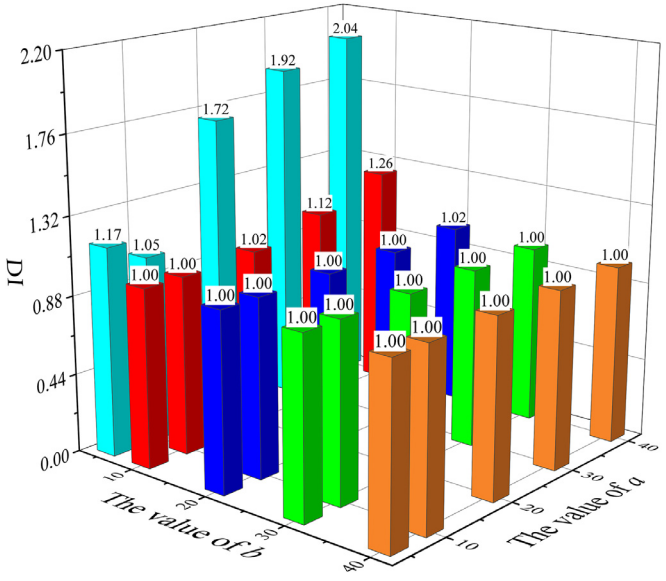

Fig. 15. The influence of a and b on DI

lines respectively, so their values may affect the stability of the detection model. Taking the data of experiment 1.4 as an example, the force curve is shown in Fig. 13 (a). After changing a and b, the results are shown in Fig. 13 - Fig. 15. It can be seen from Fig. 13 (b-d) that the values of a and b have an impact on the time delay and stability of the KR_{opt} curve.

The time delay is obtained by calculating the time difference between the actual collision point and the highest peak point of the KR_{opt} curve. As shown in Fig. 14, The time delay is positively correlated with the value of a, but has no obvious relationship with the value of b.

This paper uses a new method to express the degree of instability (DI) of the KR_{opt} curve. The calculation method of DI is given by Eq.12:

$$DI = \frac{SP-ST}{LP} \tag{12}$$

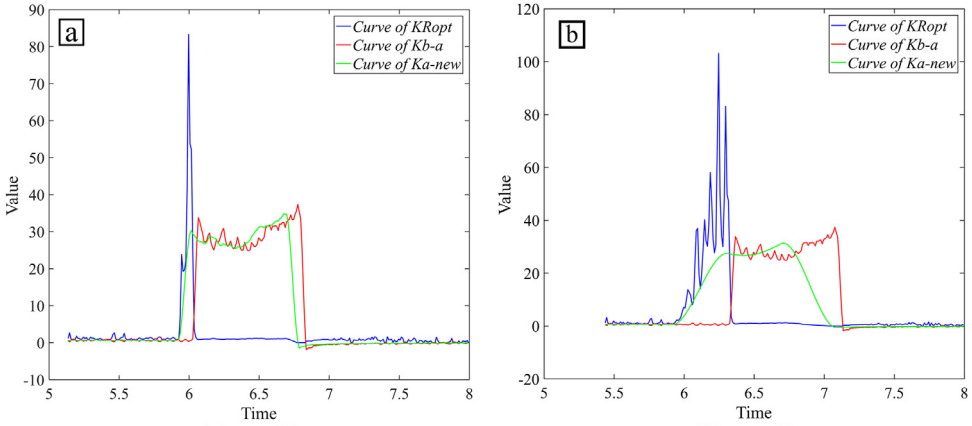

Fig. 16. KR_{opt} curve under different values of a when b=5

Where, SP is the sum of all peaks in the KR_{opt} curve, ST is the sum of all troughs, LP is the largest one among the peaks of the KR_{opt} curve. It should be noted that all calculated peak and troughs values must be greater than 5. It can be seen from the Eq.12 that the greater the value of DI, the greater the difference between the peak and the trough of the KR_{opt} curve, and the greater the volatility of the curve. When DI=1, it means that the KR_{opt} curve has only one peak and the performance is the best. As seen from Fig. 15, DI is mainly influenced by the value of b. When the value of b is less than 30, the increase of a will increase the instability of the system. This is because an increase in a will make the $K_{a\text{-}new}$ curve too far ahead of the $K_{b\text{-}a}$ curve. When the value of $K_{a\text{-}new}$ has risen to a large value, but the value of $K_{b\text{-}a}$ is still small and fluctuates greatly, the fluctuation degree of $K_{a\text{-}new}/K_{b\text{-}a}$ will be large, as shown in Fig. 16. Therefore, the cause of the problem is still that b is too small and the $K_{b\text{-}a}$ curve is unstable. Increasing b can solve this problem. The value of a and b should be selected according to the needs of the system. When the system has high requirements for real-time and reliable detection, a=5 and b=40 can meet the requirements.

5. Conclusion

In this paper, a mechanical model of fracture bone collision based on three element viscoelastic model was established, and a collision detection model was further constructed based on the slope ratio of force curve. The factors that affect the slope of the collision force curve were analyzed through the broken bone collision mechanics model. The effects of these factors on the slope of the force curve and its ratio were explored through experiments. The experimental results show that the slope ratio decreases with the increase of reduction speed and soft tissue mass, and increases with the increase of collision angle. Excluding the influence of soft tissue stiffness, the collision area has little effect on the slope ratio. According to the force curve obtained from the above single factor experiments, the availability of the established collision detection model and the necessity of optimization was verified. The collision of broken bones can be judged by setting the detection threshold. Through the analysis of the performance of the detection model, it was found that a smaller a value and a larger b value could improve the comprehensive performance of the detection model.

The collision mechanical model and collision detection model established in this paper have reference value for improving the safety of robot assisted fracture reduction system. But the research is based on vitro experiments. The actual fracture reduction process is more complex, which may challenge the application of this model. It should be noted that this article only explored the influence of the main factors on the slope ratio according to Eq.7, and didn't consider the influence of more complex factors such as the fracture position and the shape of the fracture on the detection results. In addition, the collision surface was also polished to reduce the influence of the change of friction coefficient on the experimental results. This may cause the experimental results to have a certain deviation compared with the actual application. In the follow-up research, a real-time collision detection system will be built based on the detection model, and be optimized through animal carcass experiments.

Declaration of Competing Interest

The authors declare no conflict of interest.

Acknowledgments

This work was supported by the National Natural Science Foundation of China (52075301), the National Key R&D Program of China (2019YFC0119200), the Key R&D Program of Shandong Province (2019GHZ002) and the Natural Science Foundation of Shandong Province (ZR2019MEE017).

Reference

[1] L Bai, J Yang, X Chen, et al., Medical Robotics in Bone Fracture Reduction Surgery: A Review, Sensors 19 (16) (2019) 3593, doi:10.3390/s19163593.
[2] J X Zhao, C Li, H Ren, et al., Evolution and Current Applications of Robot-Assisted Fracture Reduction: A Comprehensive Review, Ann. Biomed. Eng. 48 (1) (2020) 203–224, doi:10.1007/s10439-019-02332-y.
[3] Y A Weil, A Greenberg, A Khoury, et al., Computerized navigation for length and rotation control in femoral fractures: a preliminary clinical study, J. Orthop. Trauma. 28 (2) (2014) E27–E33, doi:10.1097/BOT.0b013e31829aaefb.
[4] G Dagnino, I Georgilas, P Khler, et al., Navigation system for robot-assisted intra-articular lower-limb fracture surgery, Int. J. Comput. Ass. Rad. 11 (10) (2016) 1831–1843, doi:10.1007/s11548-016-1418-z.
[5] B Vibert, R Pailhe, V Morin, B Rubens-Duval, D Saragaglia, Navigation for lower limb alignment during internal fixation of complex tibial-plateau fractures, Orthop. Traumatol-Sur. 104 (4) (2018) 491–496, doi:10.1016/j.otsr.2018.03.006.
[6] S Pflugi, L Li, T M Ecker, et al., A Cost-Effective Surgical Navigation Solution for Periacetabular Osteotomy (PAO) Surgery, Int. J. Comput. Ass. Rad. 11 (2) (2016) 271–280, doi:10.1007/s11548-015-1267-1.
[7] G Zheng, X Dong, P A Grutzner, et al., Automated detection and segmentation of cylindrical fragments from calibrated C-arm images for long bone fracture reduction, Comput. Meth. Prog. Bio. 87 (1) (2007) 1–11, doi:10.1016/j.cmpb.2007.03.002.
[8] J Buschbaum, R Fremd, T Pohlemann, et al., Computer-assisted fracture reduction: a new approach for repositioning femoral fractures and planning reduction paths, Int. J. Comput. Ass. Rad. 10 (2) (2015) 149–159, doi:10.1007/s11548-014-1011-2.
[9] Du Hailong, Lei, et al., Preoperative trajectory planning for closed reduction of long-bone diaphyseal fracture using a computer-assisted reduction system, Int. J. Med. Robot. Comp. 11 (1) (2015) 58–66, doi:10.1002/rcs.1573.

[10] M Bhandari, T Zeffiro, M. Reddiboina, Artificial intelligence and robotic surgery: current perspective and future directions, Curr. opin. urol. 30 (1) (2020) 48–54, doi:10.1097/MOU.0000000000000692.
[11] S Guo, M J Yang, J. Tan, A Big Challenge of Surgical Robot-Haptic Feedback, Chin. J. Bio. Eng. 32 (4) (2013) 499–503, doi:10.3969/j.issn.0258-8021.2013.04.017.
[12] S Guo, Y Wang, N Xiao, et al., Study on real-time force feedback for a master–slave interventional surgical robotic system, Biomed. Microdevices 20 (2) (2018) 1–10, doi:10.1007/s10544-018-0278-4.
[13] B Zhao, CA. Nelson, A sensorless force-feedback system for robot-assisted laparoscopic surgery, Comput. Assist. Surg. 24 (sup1) (2019) 36–43, doi:10.1080/24699322.2018.1557887.
[14] JS Kang, MC Lee, SM. Yoon, Bilateral control based rupture protection method in surgical robot using improved master device, Int. J. Control Autom. 14 (4) (2016) 1073–1080, doi:10.1007/s12555-014-0555-9.
[15] C Li, T Wang, L Hu, et al., A novel master–slave teleoperation robot system for diaphyseal fracture reduction: a preliminary study, Comput. Assist. Surg. 21 (sup1) (2016) 162–167, doi:10.1080/24699322.2016.1240304.
[16] M Wang, L Sun, Z Du, et al., in: The design and implementation of virtual system for the robot-assisted setting-bone surgery, 2006 Bio Micro and Nanosystems Conference, San Francisco, USA, 2006, pp. 53–57, doi:10.1109/BMN.2006.330928.
[17] T Gösling, R Westphal, J Faülstich, K Sommer, F Wahl, C Krettek, T. Hufner, Forces and torques during fracture reduction: intraoperative measurements in the femur, J. Orthop. Res. 24 (3) (2006) 333–338, doi:10.1002/jor.20045.
[18] N Fan, S Yuan, P Du, et al., Design of a robot-assisted system for transforaminal percutaneous endoscopic lumbar surgeries: study protocol, J. Orthop. Surg. Res. 15 (1) (2020) 1–7, doi:10.1186/s13018-020-02003-y.
[19] R Xue, B Ren, J Huang, et al., Design and evaluation of FBG-based tension sensor in laparoscope surgical robots, Sensors 18 (7) (2018) 2067, doi:10.3390/s18072067.
[20] J. Buschbaum, R. Fremd, T. Pohlemann, A. Kristen, Introduction of a computer-based method for automated planning of reduction paths under consideration of simulated muscular forces, Int. J. Comput. Ass. Rad. 12 (8) (2017) 1369–1381, doi:10.1007/s11548-017-1562-0.
[21] Q Li, R Song, X Ma, et al., Collision Localization Algorithm for Surgical Robots Fusing Image and Force Data, J. Med. Imag. Health In. 9 (4) (2019) 824–829, doi:10.1166/jmihi.2019.2678.
[22] W Y Kim, S Y Ko, J O Park, et al., 6-DOF force feedback control of robot-assisted bone fracture reduction system using double F/T sensors and adjustable admittances to protect bones against damage, Mechatronics 35 (2016) 136–147, doi:10.1016/j.mechatronics.2016.02.005.
[23] D Fyhrie, B. Christiansen, Bone Material Properties and Skeletal Fragility, Calcified Tissue Int. 97 (3) (2015) 213–228, doi:10.1007/s00223-015-9997-1.
[24] M S Sacks, W. Sun, Multiaxial Mechanical Behavior of Biological Materials, Annu. Rev. Biomed. Eng. 5 (1) (2003) 251–284, doi:10.1146/annurev.bioeng.5.011303.120714.
[25] M. Sato, Mechanical properties of living tissues, Iyō Denshi to Seitai Kōgaku Japanese J. Med. Electronics Biol. Eng. 24 (4) (1986) 213–219, doi:10.11239/jsmbe1963.24.213.
[26] SA. Glantz, A three-element description for muscle with viscoelastic passive elements, J. Biomech. 10 (1) (1977) 5–20, doi:10.1016/0021-9290(77)90025-2.